Fuel Processing Technology 237 (2022) 107475

Contents lists available at ScienceDirect

Fuel Processing Technology

journal homepage: www.elsevier.com/locate/fuproc

Lab-scale experimental demonstration of Ca—Cu chemical looping for hydrogen production and in-situ CO_2 capture from a steel-mill

Syed Zaheer Abbas [a], José Ramón Fernández [b], Alvaro Amieiro [c], Monisha Rastogi [d], Johan Brandt [d], Vincenzo Spallina [a,*]

[a] Department of Chemical Engineering, University of Manchester, Sackville Street, M13 9PL, Manchester, United Kingdom
[b] Instituto de Ciencia y Tecnologia del Carbono, CSIC-INCAR, Francisco Pintado Fe, 26, Oviedo 33011, Spain
[c] Johnson Matthey Technology Centre, Reading RG4 9NH, United Kingdom
[d] Carmeuse Research and Technology, Louvain-la-Neuve 1348, Belgium

ARTICLE INFO

Keywords:
Calcium-copper looping
Steel mill
Blast furnace gas
CO_2 capture
Chemical looping combustion

ABSTRACT

In the present work, a lab-scale packed bed reactor has been used to decarbonize mixtures of inlet gases simulating the typical composition of blast furnace gases (BFG) and convert them to H_2-rich streams by means of the Ca—Cu chemical looping concept. The reactor was packed with 355 g of Cu-based oxygen carrier (OC) supported on Al_2O_3 and natural Ca-based sorbent. The three main reaction stages; namely (i) Calcium Assisted Steel-mill Off-gas Hydrogen (CASOH), (ii) Cu oxidation and (iii) Regeneration of carbonated Ca-based sorbent were examined. In CASOH stage, BFG is converted into H_2-rich stream (17% by vol.) under the experimental conditions of 600 °C, 5.0 bar and S/CO molar ratio of 2.0. A controlled oxidation causes a mere 3.5% of $CaCO_3$ to decompose during the Cu-oxidation stage. This resulted in a nearly pure N_2 stream at 600 °C and 5.0 bar operating conditions. During the regeneration stage, BFG and mixture of BFG and CH_4 is used as a reducing fuel. To ensure the amount of heat needed for the decomposition of $CaCO_3$ during the reduction of CuO, a 1.4 CuO/$CaCO_3$ molar ratio has been used. It resulted in 46% CO_2 in N_2 at the end of the reduction/calcination stage.

1. Introduction

Roughly, 20% of global CO_2 emission is due to the burning of fossil fuels in the heavy chemical industries such as iron and steel (31%), cement (27%), refineries (10%) and other petrochemical industries (32%). These heavy chemical industries release 10 Gt_{CO2} into the atmosphere annually [1]. Steel production is predicted to exceed 2200 Mt. a year in 2050, causing a considerable rise in energy consumption and CO_2 emissions. In these conditions, even the best possible energy-efficiency techniques would not be able to reduce the emission of CO_2 to the level set for the future (carbon neutral by 2050) [2]. Therefore, there is a need to develop and implement CCUS techniques for CO_2 reduction in the steel sector. In steel industry, the two major routes responsible for steel production are; (i) the blast furnace (BF) and basic oxygen furnace (BOF) integrated route (BF/BOF), which represents nearly 65% of the world steel production and (ii) electric arc furnace (EAF) route, which contributes nearly 35% of the world steel production [3,4]. The blast furnace gas (BFG) has very low heating value (LHV = 2–4 MJ kg^{-1}), and a very high carbon content (> 45% by vol.). Therefore, it is important to develop CO_2 capture technologies to decarbonize existing steel plants and when possible, upgrade BFG into a valuable low carbon-fuel for energy and chemical uses.

In the present scenario, three routes/viable solutions have emerged as the best possible routes for the zero carbon emission in steel industry [5] namely: (i) switching from coke as a reducing agent to H_2, (ii) implementation of carbon capture and storage (CCS) technologies and (iii) using biomass rather than coal as a reducing agent and source of energy. Several CCS technologies are sufficiently mature and ready to use with ideally zero carbon emission from steel industries. Pre- and post-combustion CCS technologies are widely used for retrofitting of existing plants. The monoethanolamine (MEA) based post-combustion process is a chemical absorption process widely used in industrial sector to reduce the level of CO_2 in the off-gases. However, the high content of CO_2 in the BFG demands for a high consumptions of steam, required for the regeneration of the absorbent, hence, causes a limited application in the steel industries [6–8]. The pre-combustion capturing of CO_2 with methyldiethanolamine (MDEA) requires more modification in the existing plant as compared to the post-combustion with MEA.

* Corresponding author.
E-mail address: vincenzo.spallina@manchester.ac.uk (V. Spallina).

https://doi.org/10.1016/j.fuproc.2022.107475
Received 8 June 2022; Received in revised form 3 August 2022; Accepted 22 August 2022
Available online 5 September 2022

However, with this process nearly 90% CO_2 can be avoided in the off-gases [9]. The amine-based sorbents having a high CO_2 capture capacity and improved durability have been developed during the VALORCO project [10], and this technology is being tested at Technology readiness level-7 (TRL7) for steel mill off-gases in the framework of the ongoing 3D Project [11,12]. In the H2020 STEPWISE project, the low heating value BFG is transformed into a H_2-rich gas having >30% vol. H_2 by reacting with steam through a water-gas shift process (WGS), whereas the CO_2 produced during the reaction is captured by the hydrotalcite-based sorbent [13]. The demonstration of this technology up to TRL6–7 has been carried out during the consecutive EU programmes CACHET, CAESAR, and STEPWISE [14]. A wide range of additional emerging CO_2 capture technologies have been proposed to target gas streams in the iron and steel industries, either as post-combustion or as a top gas recycle concepts (advanced solvents [15], membranes [16], new solid sorbents for Pressure Swing Adsorption and Vacuum Pressure Swing Adsorption (PSA/VPSA) [17], chemical looping and calcium looping [18,19]). All these technologies present issues regarding stability of functional materials, role of impurities, energy consumption, retrofitability and need of rigorous quantitative estimation of cost and overall process efficiencies.

The Ca-based materials have also been widely proposed as CO_2-sorbents in various pre-combustion applications [20,21] [22], they theoretically allow process intensification by conducting several reactions steps in a single reactor and can yield high theoretical energy efficiencies because their operating conditions at suitably high temperatures. However, the development of these processes have encountered serious issues, as a very high temperature (~900 °C) is required during the regeneration of the used sorbent to produce a CO_2 rich gas stream. Despite of having an advantage of recovering thermal energy input during the carbonation and heat removal stages, there is still a main challenge of providing a thermal heat during the regeneration stage. To counter this issue, one feasible solution is to merge the sorption-enhanced process and the chemical looping combustion (CLC) of metal oxides. During the Ca—Cu chemical looping process, the reduction of CuO using a various gaseous fuel such as CH_4, CO, or H_2 provides the necessary heat for the calcination of the carbonated sorbent resulted in producing CO_2 and H_2O without the need of any air separation unit (ASU) [23]. In EU ASCENT project, a considerable development was made on reactor modelling [24,25] with the preparing and characterization of Ca—Cu materials [25], process integration [26,27], and lab-scale to TRL5 scale validation of packed beds reactor [28–30]. The application of Ca—Cu chemical process in steel-mills to produce H_2 and CO_2 rich using interconnected fluidized bed reactors have been widely proposed in literature [18,31]. The arrangement of interconnected fluidized bed reactor not only helps in assisting the heat management in the highly exothermic redox stages, but it also results in a continuous production of desirable product streams. However, this setup has a pressure restrictions and needs an extra unit to separate the Ca- from the Cu-based materials once the sorbent has been completely regenerated. In a previous work [32], a variant of these processes has been proposed using packed bed reactors to conceptually design the Calcium Assisted Steel-mill Off-gas Hydrogen (CASOH) production process (Fig. 1) based on the concept of pre-combustion capture with Calcium Assisted WGS to capture the CO_2 at the downstream of BF in a steel plant. In the proposed CASOH process, BFG is transformed into a H_2-rich stream free of CO_2 with higher Lower Heating Value (LHV) while producing a large amount of high-temperature heat. The process is carried out in dynamically operated packed-bed reactors following a set of three main reaction stages: CASOH, Cu oxidation and regeneration as shown in Fig. 1. The main reactions considered in the CASOH process are illustrated in Table 1.

The conditions of temperature and pressure are changed to facilitate the conditions of the solids bed in each stage, following well established principles of PSA/TSA and regenerative heat-transfer processes [32]. In the present work, we have used the combined Ca—Cu based material in a packed bed reactor to study the main reaction stages (CASOH stage, Cu-oxidation stage and reduction/calcination stage) occurring during the CASOH process. Prior to the CASOH experimentation, the individual Ca- and Cu-based materials are tested under the various temperature (400–850 °C) and pressure (1–5 bar) conditions for over 300 h of operation. The CASOH experiments are carried out in a packed bed reactor under the different conditions of temperature (600–870 °C), pressure (1–5 bar), flowrate of feed (10–20 NLPM) and inlet gas compositions. A lot of research has been carried out on sorption enhanced WGS and sorption enhanced reforming, as well as chemical/Calcium looping technology applied to H_2 production. Despite the research proposed in that area does not refer to integrated steelmill [30,33–41]. The pseudo-continuous CASOH process in a lab-scale packed bed reactor under high-pressure conditions is demonstrated first time in the literature. Apart from the testing of the gas-solid combined chemical/calcium looping above atmospheric pressure and flowrate which has never been presented in literature confirming several of the hypotheses previously formulated but never demonstrated, this work is also looking at the process operation by using existing material paving the way to the further scale-up and demonstration.

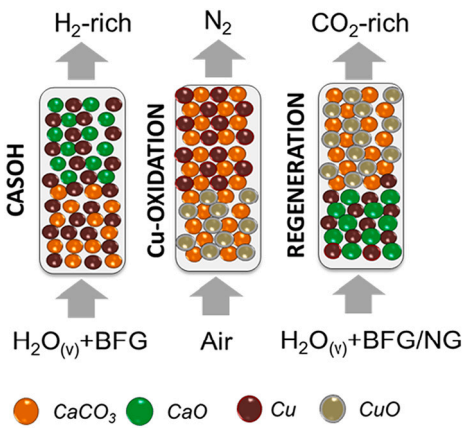

Fig. 1. Scheme of the CASOH process for the conversion of LHV BFG to H_2 and CO_2 rich streams ready for the subsequent storage or utilization.

2. Process description

In the CASOH stage, the 20% vol. CO present in the BFG reacts with the steam through the WGS reaction (R7) and produces a H_2/N_2 fuel gas. The Cu acts as a catalyst during the WGS reaction and the CaO reacts with CO_2 forming $CaCO_3$ (R1). The continuous removal of the formed CO_2 from the gas phase shifts the WGS equilibrium towards a higher H_2 production (about 34%, on a dry basis), therefore, it is feasible to have a higher CO conversion under the operating conditions of 600 °C to 650 °C and 5.0 bar, and consequently <1% of CO is present in the product gas. Once the CaO-based reaches to its full saturation, and the further conversion of BFG to H_2/N_2 is no longer possible in the CASOH stage, the reactor would act as a stationary WGS unit. In the second step of the process, the Cu-based particles are oxidized (R3) using air at high pressure and moderate temperatures (i.e. at 5.0 bar and temperatures below 650 °C) to minimize the calcination of $CaCO_3$, thereby leading to a negligible carbon leakage during this operation. Finally, in the third reaction stage, the exothermic reduction of CuO to Cu (R4 – R6) using BFG, other steel mill off-gases or natural gas (NG) provides the necessary heat for the calcination of the spent sorbent (R2). This is a unique feature of the process, because by exploiting the exothermic reduction of CuO to Cu it is possible to produce a CO_2-rich gas (exclusively CO_2 and H_2O if a N_2-free fuel gas is used) during the CO_2 sorbent regeneration by calcination. To carry out the sorbent regeneration in the CASOH process and produce a rich stream in CO_2, an atmospheric pressure is needed to facilitate the decomposition/calcination of the $CaCO_3$ at a moderate

Table 1
Main reactions considered in CASOH process.

Process	Reaction		
Carbonation	$CaO_{(s)} + CO_{2(g)} \rightarrow CaCO_{3(s)}$	ΔH_{298K} = -178.8 kJ mol^{-1}	(R1)
Calcination	$CaCO_{3(s)} \rightarrow CO_{2(g)} + CaO_{(s)}$	ΔH_{298K} = 178.8 kJ mol^{-1}	(R2)
Oxidation of Cu	$2\ Cu_{(s)} + O_{2(g)} \rightarrow 2\ CuO_{(s)}$	ΔH_{298K} = -310.4 kJ mol^{-1}	(R3)
Reduction of CuO	$CuO_{(s)} + H_{2(g)} \rightarrow Cu_{(s)} + H_2O_{(g)}$	ΔH_{298K} = -86.6 kJ mol^{-1}	(R4)
	$CuO_{(s)} + CO_{(g)} \rightarrow Cu_{(s)} + CO_{2(g)}$	ΔH_{298K} = -127.8 kJ mol^{-1}	(R5)
	$4\ CuO_{(s)} + CH_{4(g)} \rightarrow 4\ Cu_{(s)} + 2\ H_2O_{(g)} + CO_{2(g)}$	ΔH_{298K} = -181.5 kJ mol^{-1}	(R6)
Water gas shift (WGS)	$CO_{(g)} + H_2O_{(g)} \rightarrow H_{2(g)} + CO_{2(g)}$	ΔH_{298K} = -41.2 kJ mol^{-1}	(R7)

temperature (below 900 °C), according to the equilibrium data of CaO/$CaCO_3$ [23,42]. A suitable CuO/$CaCO_3$ molar ratio of active Ca and Cu components in the composition of the bed will ensure that the heat released during the reduction of CuO is sufficient to completely decompose the $CaCO_3$ without any external energy supply [43].

3. Methodology

3.1. Experimental setup

The CASOH process experimental campaign has been conducted in a laboratory setup located in the James Chadwick Building (JCB) at the University of Manchester. The state-of-the art laboratory setup is divided into two fume cupboards (FC), i.e. fume cupboard-1 (FC-1) and fume cupboard-2 (FC-2) as demonstrated in Fig. 2**(a – c)**. In the FC-1, the inlet dry gases feeding system and the product gas analysis equipment such as a Hiden QGA mass spectrometer and a Siemens CO analyser, are located. The gas feeding system comprises of a central supply of H_2, CH_4, N_2, He, air and in-house cylinders of CO and CO_2 as shown in Fig. 2**(a)**. The feed flowrates and pressure are regulated and controlled by the Bronkhorst mass flow controllers and a Bronkhorst pressure controller respectively. The FC-2 has a packed-bed reactor setup (manufactured by Array Industries B·V) having an inside diameter of 35 mm and a total reactor length of 1050 mm as shown in Fig. 2**(b)**. The reactor is enclosed in a Carbolite furnace. Inside the reactor, a thermowell having 10 K-type thermocouples (TC) measures the temperature along the length of the bed. Each TC is 45 mm apart from each other. A schematic of the packed bed reactor is shown in Fig. 2**(c)**. An HPLC pump (LC-20AP Shimadzu) is used to deliver the water into a Carbolite steam generator, which can operate from 30 to 3000 °C. The outlet of steam generator, reactor inlet and outlet are insulated and heated using heating tape. The reactor exhaust gases are cooled in an ice-bath to ensure that no water content is sent to the gas analysis units.

Fig. 3 represents the overall P&ID of the experimental setup. An in-house HMI system is used to control the flow rate and pressure conditions. The HMI system also records the temperatures at the multiple

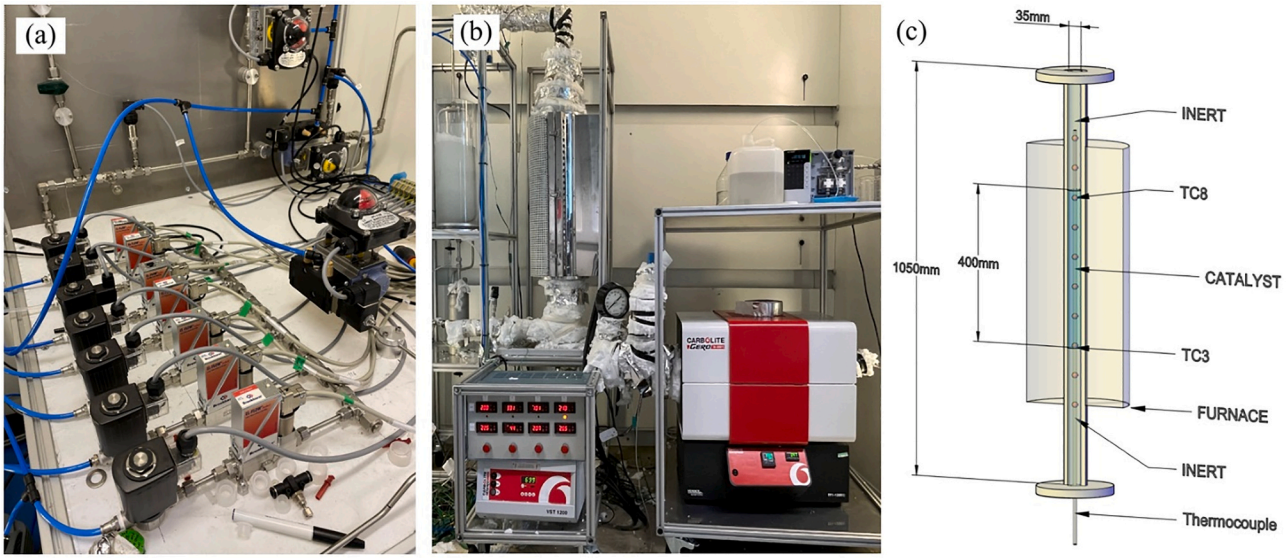

Fig. 2. The TRL4 packed bed reactor set-up located at the University of Manchester having (a) an inlet dry gas feeding system in FC-1; (b) a packed-bed reactor enclosed in a furnace placed in FC-2 and (c) schematic diagram of the packed-bed reactor unit.

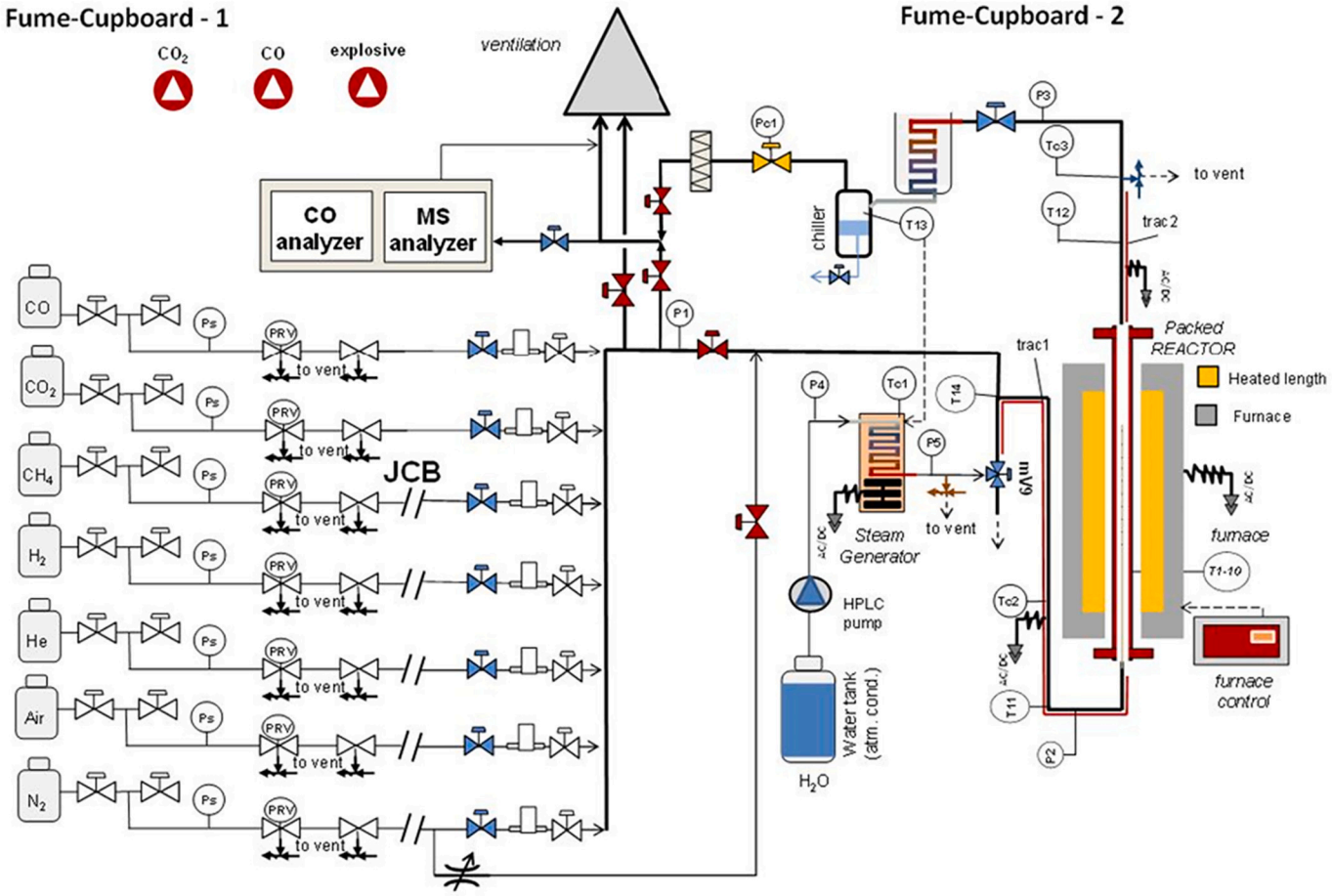

Fig. 3. The overall P&ID diagram of the experimental setup.

detection points of the thermocouples. In addition, a second independent HMI unit was used to monitor the gas compositions obtained through the MS and the CO analyser.

In this experimental campaign, a mixture of 205 g Ca-based material supplied by Carmeuse and 150 g of Cu-based material supplied by Johnson Matthey, as shown in Fig. 4, was crushed to get an average particle size of 1.5–2 mm using Pulverized Ball mill and loaded in the reactor. Despite natural ore CaO exhibits low reactivity compared to new and more performing Ca-based sorbent, in this this study we tested existing material available from lime production which results in low-cost and high availability. The solid material amount has been chosen to make sure that we do not require any external heat supply during the CaO regeneration stage. To make sure the Ca—Cu mixture is held firmed in the reactor, the bottom and top section of the packed bed reactor was packed with an inert material (Al_2O_3), having a particle size of 3 mm. The solids bed length was 400 mm. The Ca—Cu mixture is tested for various consecutive cycles of CASOH, oxidation and reduction/calcination at the conditions listed in Table 2. The intermediate cooling and/or heating stages were used to avoid any undesired reaction in between the process stages and to prepare the bed for the subsequent stage with a controlled initial solid temperature. Prior to the CASOH process experimentation, Cu- and Ca-based materials are activated individually. Cu-based material was tested for 30 consecutive reduction and oxidation cycles. The redox cycles were performed at 500 °C and 1.0 bar with a 20% vol. H_2 in N_2 gas stream for the reduction reaction, while oxidation was performed with a 10% vol. O_2 in N_2 gas stream.

4. Results and discussion

4.1. Cu-based material stability testing

Before testing the combined Ca—Cu material at a TRL-4 reactor setup, the Cu-based OC was activated and tested over 30 consecutive redox cycles in the packed-bed to check the chemical stability of the material. The Cu-based material showed high reactivity resulting in very sharp breakthrough curves and highly reproducible oxidation and reduction breakthrough profiles were obtained as shown in Fig. 5.

Moreover, the oxygen transfer capacity of the material, expressed as grams of oxygen reacting per gram of material in oxidized form (OTC), remained stable along the redox cycles, as it can be seen in Fig. 6. According to the mass changes measured during the successive reduction and oxidation cycles, about 14.5–15.0% wt. Cu was reacting in the material.

4.2. Ca – based material stability testing

Prior to the combined material testing, the Ca-based material was first exposed to 10 calcination/carbonation cycles until the residual CO_2 sorption capacity was achieved. The carbonation process was performed with the solids bed initially at 600 °C with 20% vol. CO_2 in N_2, whereas the calcination stage was carried out at 900 °C in N_2. Fig. 7 shows the CO_2 breakthrough curves and CaO conversion over 10 cycles of carbonation. The decrease in CO_2 breakthrough time over the multiple cycles indicates that the sorbent is reducing its CO_2 carrying capacity, hence, a decrease in CaO conversion as can be seen in Fig. 7 (b).

Fig. 4. Image of a) Cu-based material supplied by Johnson Matthey and b) Ca-based material supplied by Carmeuse.

Table 2
The experimental conditions used in the CASOH process.

Conditions	CASOH stage	Oxidation stage	Reduction/calcination stage
Temperature [°C]	600–650	600–650	800–870
Pressure [bar]	5	1–5	1.0
Steam-to-CO ratio	2.0	–	1.5
Inlet gas composition (vol %)	20%CO, 20% CO_2 and 60% N_2	10–21% O_2 in Air	1) 20%CO, 20%CO_2 and 60%N_2 2) 20%CO, 20%CO_2, 20%CH_4 and 60% N_2 3) 20%CH_4 and 80% N_2
Total volumetric flow (NLPM)	10	10	10–20

4.3. CASOH stage

As indicted in Table 2, a flow of 10 NLPM of synthetic fuel gas approaching typical BFG composition mixed with steam (S/CO molar ratio of 2) is fed into the packed-bed reactor to study CASOH stage. The bed is initially filled with the reduced Cu and CaO material. Fig. 8**(a – b)** shows the dry molar gas composition at the reactor outlet and temperature profile along the bed during the CASOH stage at 600 °C, 5.0 bar and S/CO molar ratio of 2.0. During the pre-breakthrough period ($0 < t \leq 2$ min), the CaO sorbent is fully active, the WGS (catalysed by the Cu-based solid) equilibrium is shifted towards the production of H_2 and almost all the CO and CO_2 is removed from the gas phase. During this period, a maximum concentration of 17% vol. H_2 and <1% vol. CO and CO_2 are obtained at the reactor exit. Fig. 8**(b)** presents the temperature variation during the CASOH stage along the length of the reactor. The WGS (R7; $\Delta H_{298K} = -41.2$ kJ mol^{-1}) and the CaO carbonation reaction (R1; $\Delta H_{298K} = -178.8$ kJ mol^{-1}) taking place in the CASOH stage are both exothermic in nature and result in a temperature increase along the length of the reactor with the passage of time. As the bed is progressively carbonated, the temperature instantly increases until a maximum value of 698 °C is obtained. The carbonation front advances first and a heat plateau is left behind. Once the active CaO approaches total carbonation ($t = 2$ min), the amount of H_2 in the product gases rapidly drops to 11% vol. and the amount of CO_2 increases to 29% vol. After the breakthrough (BT) period, the CO_2 sorbent is totally saturated and therefore further adsorption of CO_2 under these conditions is not possible. From that moment onwards ($t > 7.5$ min), the reactor acts as a simple WGS unit and a steady state product gases composition profile is achieved (i.e. 11% H_2, 4% CO, 29% CO_2 and 56% N_2 by vol.).

Fig. 9 shows the conversion of CO breakthrough curve and conversion profile during the CASOH stage. During the pre-breakthrough period, where the CaO-based sorbent is completely active, 100% CO conversion is achieved. In contrast, this conversion drops down to 95% in the post-breakthrough period where only WGS process is taking place. The results indicate that the system CaO/CuO is capable of converting a gas with typical BFG composition in a H_2/N_2 gas stream.

The H_2-rich gas obtained during CASOH stage could be used in the steel mill for power generation or sent to PSA to produce pure H_2 (at industrial grade). Other applications of this H_2/N_2 stream could also be the production of additional sponge iron by fuelling an auxiliary Direct Reduction of Iron, as proposed in [31], the production of NH_3, as recently proposed in the H2020 INITIATE [44], or gasoline and other liquid fuel or olefins, as proposed in H2020 FRESME [45] and SPIRE COZMOS [46].

Fig. 10 shows the CO_2 composition breakthrough curves at the exit of the reactor during the CASOH stage after 8 cycles of CASOH process under the operating conditions of 600 °C, 5.0 bar and S/CO molar ratio of 2.0. The results from consecutive cycles indicate that although the sorbent is progressively reducing its CO_2 carrying capacity [47], it is still capable of maintaining its reactivity while there is active CaO in the bed. In this way, gas product composition is not determined by the amount of CaO active in the bed, but the CASOH duration is affected.

Once the CASOH stage is completed, most of the reactor bed is still at a very high temperature (approximately at 690 °C). Since the Cu oxidation is an exothermic reaction, a further increase of the solid temperature would start to release CO_2 along with the N_2, thus reducing the CO_2 capture efficiency of the overall process. In order to avoid it, a heat removal (HR-1) stage is required to remove the excess amount of accumulated heat in the reactor. Therefore, a flow of 5.0 NLPM of N_2 at 600 °C is fed into the reactor and the exit gas is cooled downstream. The amount of heat recovered through the exit gas in this stage can be used at a large scale as a heat source for other units of the steelwork or it can be used to produce high-pressure (HP) steam that can later be used for the power generation.

4.4. Cu-oxidation stage

Once HR-1 has been accomplished, (i.e. the bed is at 600 °C), the oxidation stage is tested at high pressure (5.0 bar) using various O_2 concentration (10% - 21%) in the feed, as listed in Table 2. At the start of this stage, the CaO based sorbent is carbonated and the Cu-based material is present in the reduced form. The objective of the oxidation stage is to oxidize the Cu without decomposing the $CaCO_3$.

Fig. 11**(a)** shows the O_2 and CO_2 breakthrough curves during the Cu-oxidation over 30 consecutive cycles performed at 600 °C, 5.0 bar and 10% O_2 in the feed. The O_2 and CO_2 profiles are highly reproducible, which demonstrates the great stability of the Cu-based material. The

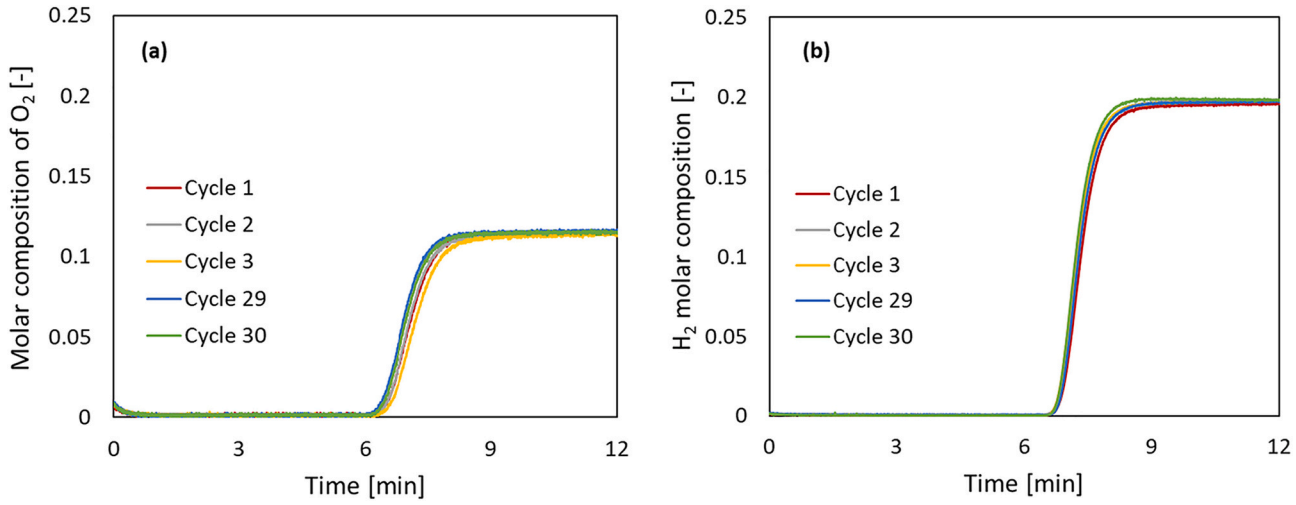

Fig. 5. Evolution of O_2 breakthrough curves during the Cu oxidation (a) and H_2 breakthrough curves during the CuO reduction (b) at 500 °C and 1.0 bar over 30 cycles. Oxidation at 10% vol. O_2 in N_2 and reduction at 20% H_2 in N_2.

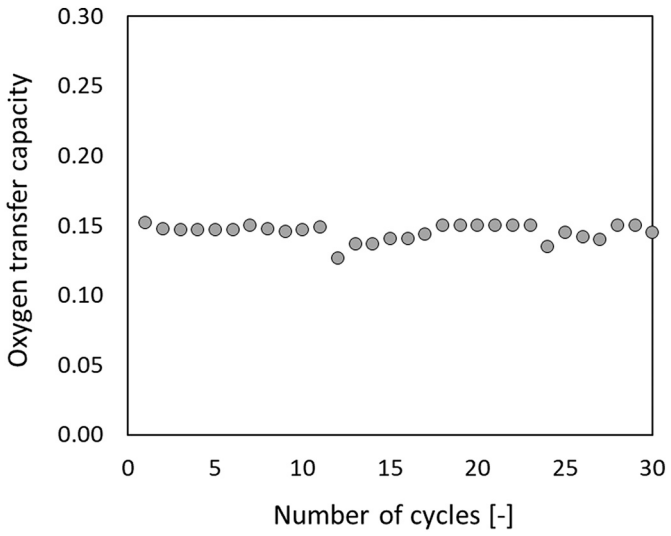

Fig. 6. Cu-based material oxygen transfer capacity (OTC) over the 30 consecutive redox cycles.

high pressure during the oxidation of Cu to CuO limits the leakage of CO_2 by partial calcination of $CaCO_3$. A maximum of 0.6% of CO_2 is observed in the product gas after 5 min of operation. The amount of CO_2 measured during the oxidation indicates that only 3.5% of the calcium carbonate present in the bed is calcined. As the O_2 is totally converted, the product gas during the pre-breakthrough period consists almost of pure N_2.

Fig. 11**(b)** illustrates the temperature profile along the length of the reactor during the Cu-oxidation. The highly exothermic reaction of Cu oxidation causes a rise in temperature of the bed to 712 °C. This temperature increase is due to the 15% by wt. of active Cu present in the reactor.

4.4.1. *Effect of temperature and pressure*

The O_2 and CO_2 breakthrough curves for various temperature (600–650 °C) and pressure (1–5 bar) is presented in Fig. 12. Due to the considerable heat losses and the effect cooling of the inlet gases, the temperature across the solid bed is not uniform, with the difference between first TC and the initial bed temperature being 50–100 °C. The O_2 breakthrough time at 600 °C and 650 °C is identical but the amount of CO_2 released at 650 °C is higher (1.6% vol.) as compared to the amount of CO_2 released at 600 °C (0.6% vol.) as shown in Fig. 12**(a)**. The higher leakage of CO_2 at 650 °C is the consequence of the maximum temperature (767 °C) achieved as compared to the maximum

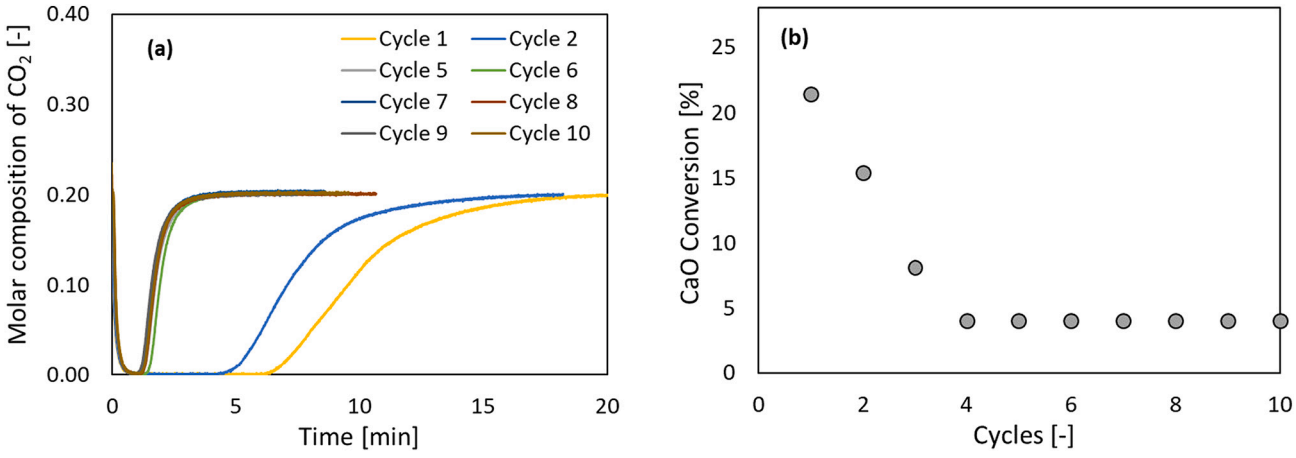

Fig. 7. a) The CO_2 breakthrough curves and b) CaO conversion (%) over multiple cycles of CaO sorption under the operating conditions of 600 °C, 5 bar and 20% CO_2 in feed.

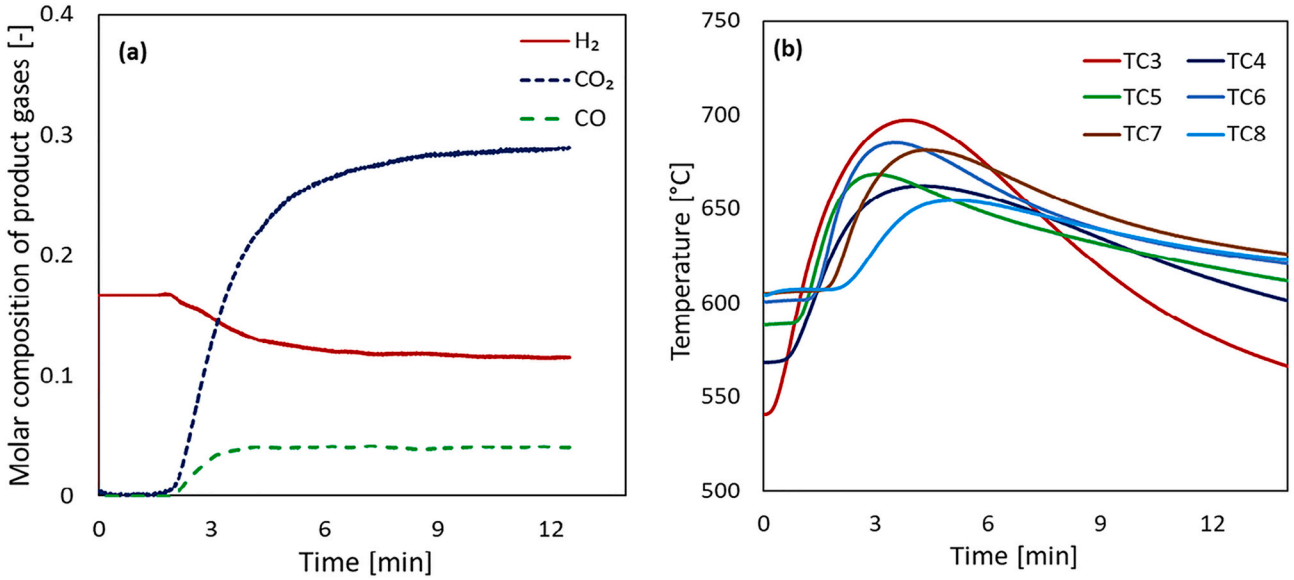

Fig. 8. a) The composition and b) reactor temperature profiles during the CASOH stage under the operating conditions of 600 °C, 5.0 bar and a feed gas composition of 20% CO_2, 20% CO, 60% N_2 and steam (S/CO ratio of 2.0).

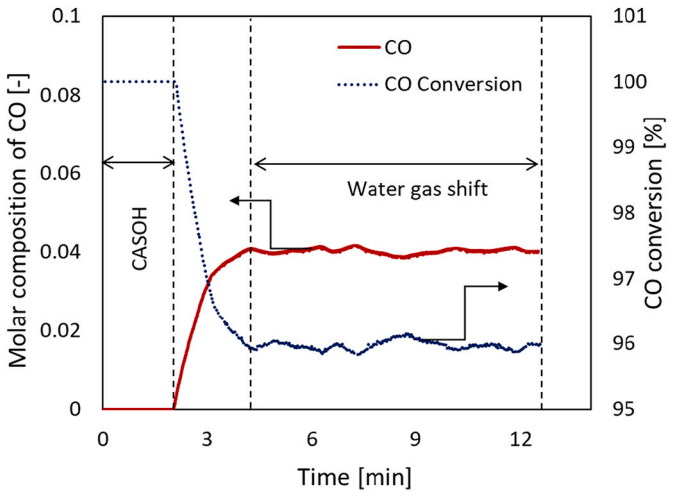

Fig. 9. The CO breakthrough and conversion profile during the CASOH stage under the operating conditions of 600 °C, 5.0 bar and a feed gas composition of 20% CO_2, 20% CO, 60% N_2 and steam (S/CO ratio of 2.0).

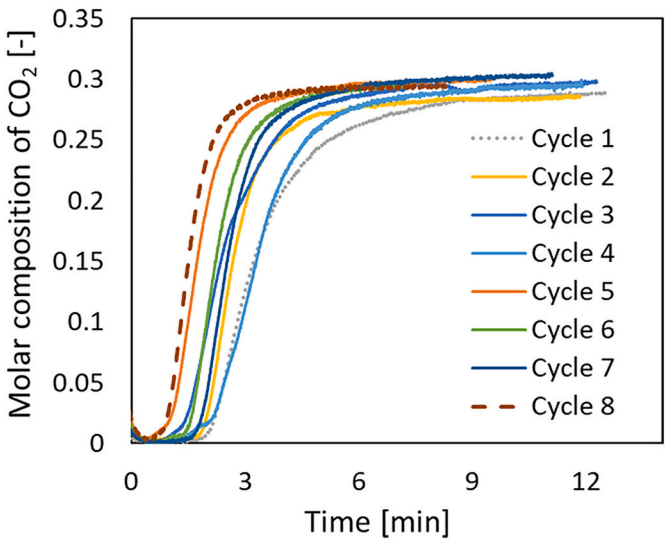

Fig. 10. The CO_2 breakthrough curves over 8 cycles of CASOH under the operating conditions of 600 °C, 5.0 bar, and a feed gas composition of 20% CO_2, 20% CO, 60% N_2 and steam (S/CO ratio of 2.0).

temperature (712 °C) achieved at 600 °C oxidation as shown in Fig. 12 **(b)**.

The decomposition of CO_2 is favourable at high temperature and low pressure as it can also be seen in Fig. 13; more CO_2 is released during the oxidation stage as we decrease the pressure from 5.0 bar to 1.0 bar under the same operating temperature and flowrate conditions. Moreover, an increase in pressure causes a later O_2 breakthrough, mainly due to 1) the decrease in gas velocity with an increase in pressure, thus resulted in increase in the gas residence time inside the reactor and 2) the strong dependency of the pressure on the kinetics [48,49].

4.4.2. *Effect of oxygen concentration*

Fig. 14 illustrates the effect of O_2 content in feed (10%, 13%, 19% and 21%) on the O_2 and CO_2 breakthrough curves during the oxidation at 600 °C, 5.0 bar and 10 NLPM conditions. As can be seen, with the increase in O_2 content, the O_2 breakthrough time decreases. Moreover, as the concentration of O_2 in the feed increases, the CO_2 concentration at the reactor outlet also increases due to the increase in the temperature in the bed, which favours the $CaCO_3$ decomposition. When feeding 21% O_2 the product gas contains 1% vol. of CO_2. However, only 0.6% vol. of CO_2 is measured when the inlet gas contains 10% of O_2.

4.5. *Reduction/calcination stage*

Once Cu is completely oxidized to CuO, the reactor is purged for 5 min with N_2 gas (5 NLPM) to eliminate any trace of O_2 in the bed and the pressure is reduced to almost atmospheric pressure to facilitate the calcination of $CaCO_3$ at temperatures below 900 °C. To avoid the calcination of $CaCO_3$ during the heating up of the reactor after the oxidation to the operating temperature of the reduction/calcination, reactor bed is heated up to the reduction/calcination temperature in 100% vol. CO_2 at atmospheric pressure. Once the calcination/reduction temperature is reached, CO_2 is tuned off and the reduction feed is introduced for the reduction and calcination reactions to take place. In

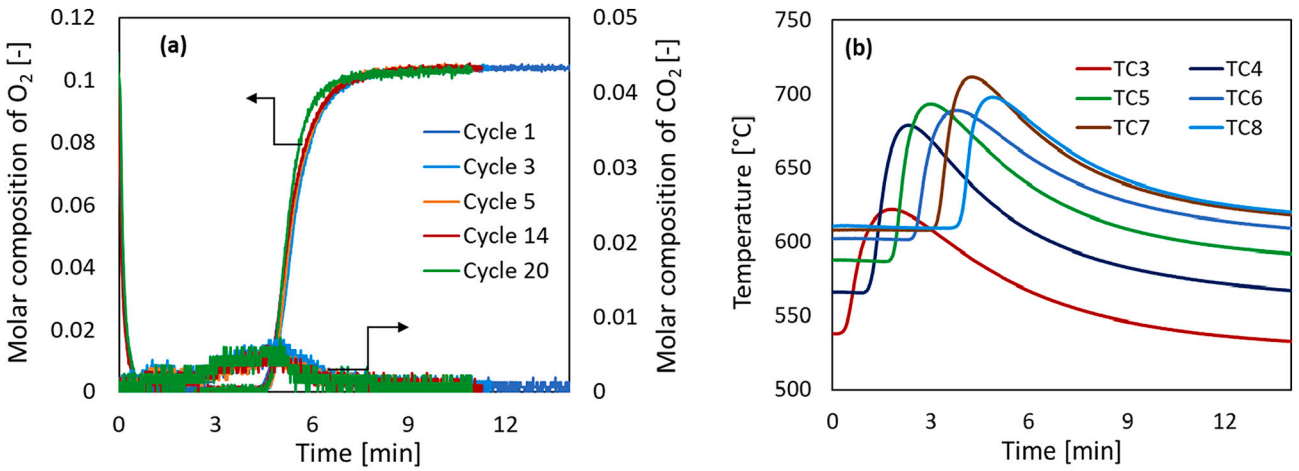

Fig. 11. a) The O_2 and CO_2 breakthrough curves over multiple cycles of Cu-oxidation; b) dynamic temperature profile during the oxidation stage under the operating conditions of 600 °C, 5.0 bar and 10% O_2 in the feed.

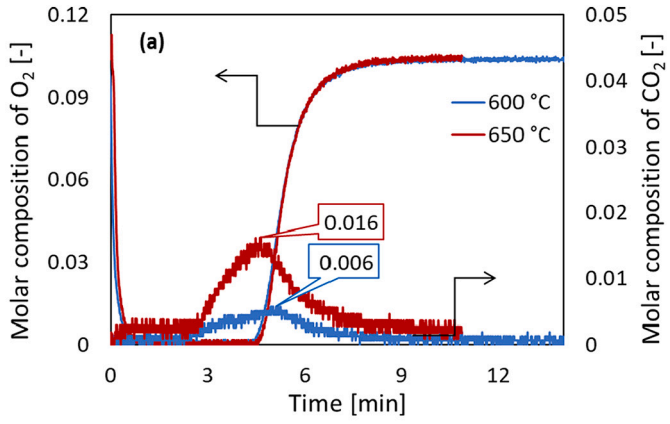

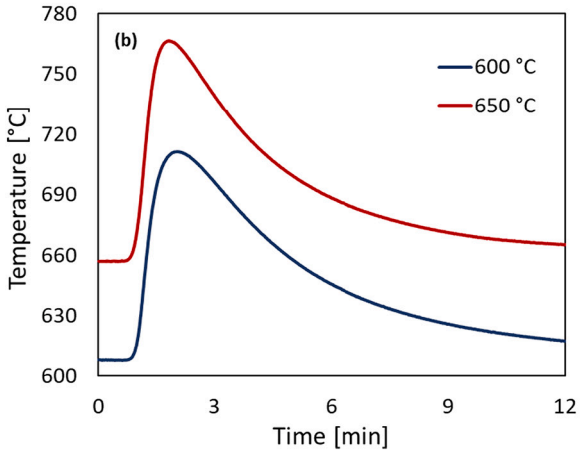

Fig. 12. a) The effect of temperature and b) the rise in temperature at TC6 during the Cu-oxidation stage using 10% O_2 in the feed.

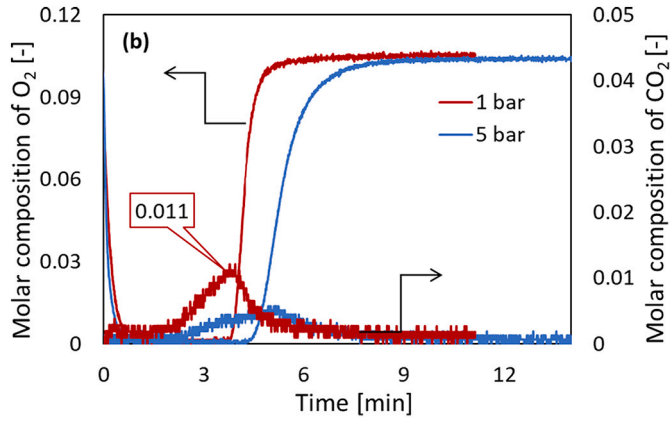

Fig. 13. The effect of pressure on the O_2 and CO_2 breakthrough curves during the Cu-oxidation stage using 10% O_2 in the feed.

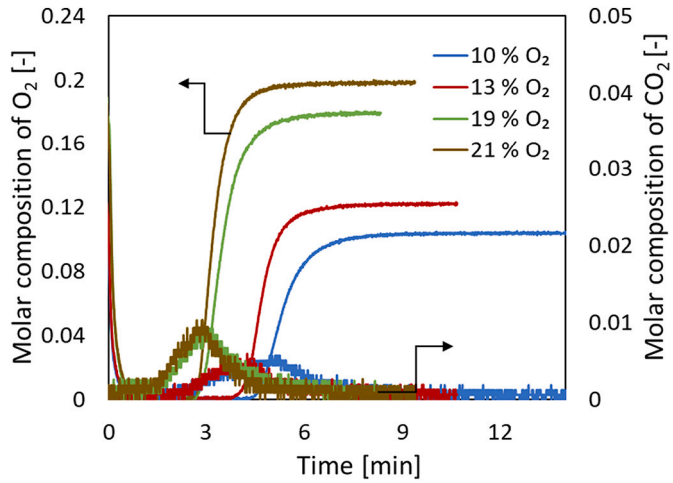

Fig. 14. The effect of O_2 concentration on the O_2 and CO_2 breakthrough curves during the Cu-oxidation stage at the operating conditions of 600 °C, 5.0 bar and a flowrate of 10 NLPM.

these conditions, the Cu/Ca molar ratio present in the solids bed is 1.4. In the rig used in this work, an initial solid temperature profile of 840–850 °C is required to achieve a final regeneration temperature of 870 °C.

Different mixtures of reducing gases and steam have been used during the reduction/calcination tests, as listed in Table 2. Fig. 15**(a)** shows the molar composition of the product gases at the outlet of the reactor during the reduction/calcination stage. When a gaseous mixture composed of 20% CO, 20% CO_2, 60% N_2 and 1.5 S/CO molar ratio is fed into the packed-bed at 800 °C a mere 10% $CaCO_3$ is calcined according

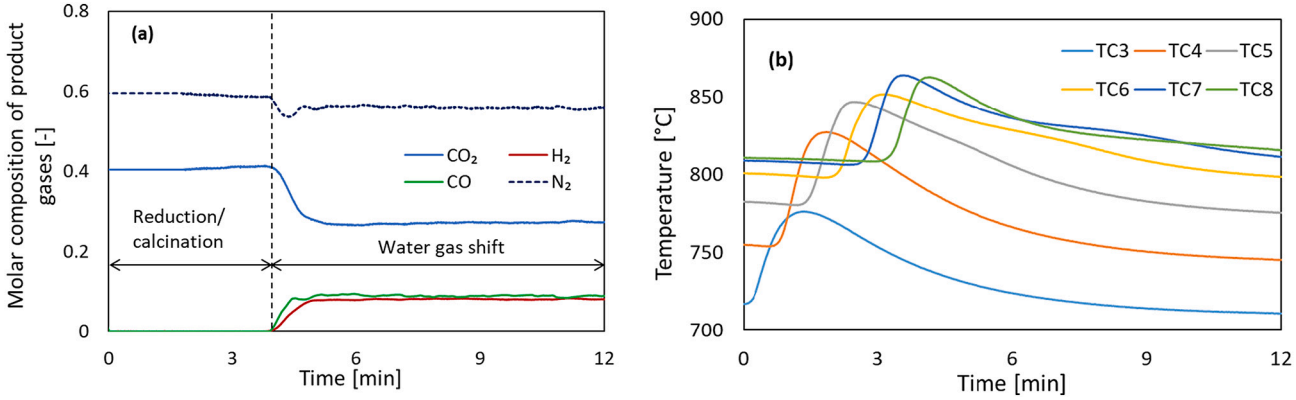

Fig. 15. a) The composition and b) solids bed temperature profiles along the length of the reactor during the reduction/calcination stage under the operating conditions of 800 °C, 1.0 bar, 20% CO_2, 20% CO, 60% N_2 and S/CO ratio of 1.5 in the feed.

to the amount of CO_2 released during the experiment. During the first 4 min of the operation, the product gas is mainly composed of 40% CO_2 and 60% N_2. Once the reduction/calcination front reaches the last portion of the bed, the CuO-based material approaches total conversion to Cu, and CO along with H_2 starts appearing in the product gas as the reactor acts as a single WGS unit. In these conditions, the temperature of the solids is insufficient and the complete calcination of $CaCO_3$ can only be achieved by heating the bed using an electric furnace. Fig. 15**(b)** shows the temperature profile with time along the length of the reactor. The sorbent calcination takes place in the region of the bed whose temperature is well above 840 °C, according to the carbonation/calcination equilibrium (i.e. P_{CO2eq}, 840 °C = 0.4).

4.5.1. Effect of solid bed temperature

To observe the effect of initial temperature on $CaCO_3$ calcination, the reduction/calcination stage has been performed between 800 °C and 870 °C at atmospheric pressure. Fig. 16 shows the product gases evolution profile at different initial temperatures in the bed (800–870 °C). The outlet composition of product gases is mainly comprised of CO_2 and N_2, as shown in Fig. 16. As the operating temperature increases, the amount of CO_2 released during the reduction/calcination is higher. In this way, the amount of CO_2 released at 870 °C corresponds to 80% calcination of $CaCO_3$ as compared to 10% and 50% calcination at 800 °C and 850 °C, respectively.

These results show that the calcination of $CaCO_3$ is favourable at higher temperature. During calcination/reduction, the heat is transferred from CuO-Cu to $CaCO_3$-CaO and the final temperature of the system is 870 °C. the heat transfer from particle-to-particle occurs fast to generate a single reaction and heat front in the reaction as shown in Fig. 15 and Fig. 16 (for the first 4 min). The same conclusions were also achieved in two previous study from CSIC [50]. Total calcination of the sorbent can be achieved by prolonging the subsequent purge with N_2 carried out at temperatures above 850 °C by further heating using electric furnace (i.e. for t < 15 min in Fig. 17).

When the calcination is carried out with synthetic BFG, a maximum concentration of 46% CO_2 diluted with N_2 is obtained. Therefore, an additional purification step is required in order to use the CO_2 or send it for storage at high purity (>95% vol.)

If CH_4 or other gases with low content of N_2 such as coke oven gas (COG) are used instead of BFG during the reduction/calcination stage, the CO_2 purification can be simplified as the only products obtained are CO_2 and H_2O. However, this scenario also causes a large additional CH_4 consumption [32]. For this reason, in this work, a gas stream containing 20% CH_4 in N_2 (**CASE 1**) and a gas mixture containing 20% CO, 20% CO_2, 20% CH_4 and 40% N_2 (**CASE 2**) along with steam ($S/CH_4 = 3$) has also been used as reducing gases for the sorbent regeneration stage. Fig. 18**(a – b)** shows higher concentrated CO_2 gas streams at the reactor exit for **CASE 1** and **CASE 2**. According to the mass balance, about 26% $CaCO_3$ is calcined using the gas mixture in **CASE 1** under the operating conditions of 800 °C and 1.0 bar. On the other hand, 64% $CaCO_3$ is calcined using the **CASE 2** gas mixture operating at 870 °C and 1.0 bar.

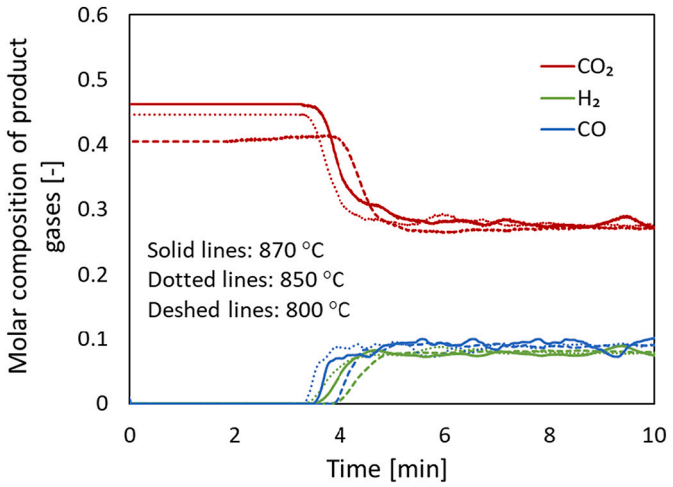

Fig. 16. The bed temperature effect on the product gas composition during the reduction stage under the operating conditions of 1.0 bar, 20% CO_2, 20% CO, 60% N_2 and S/CO ratio of 1.5 in the feed.

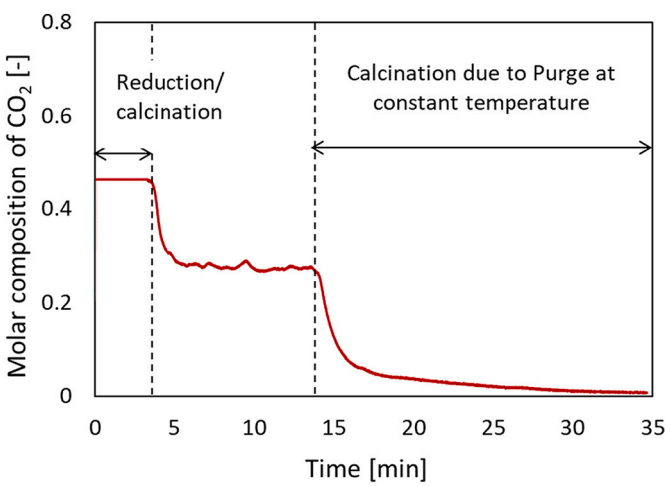

Fig. 17. The CO_2 breakthrough curve during the reduction stage under the operating conditions of 870 °C, 1.0 bar, 20% CO2, 20% CO, 60% N_2 and S/CO ratio of 1.5 in the feed.

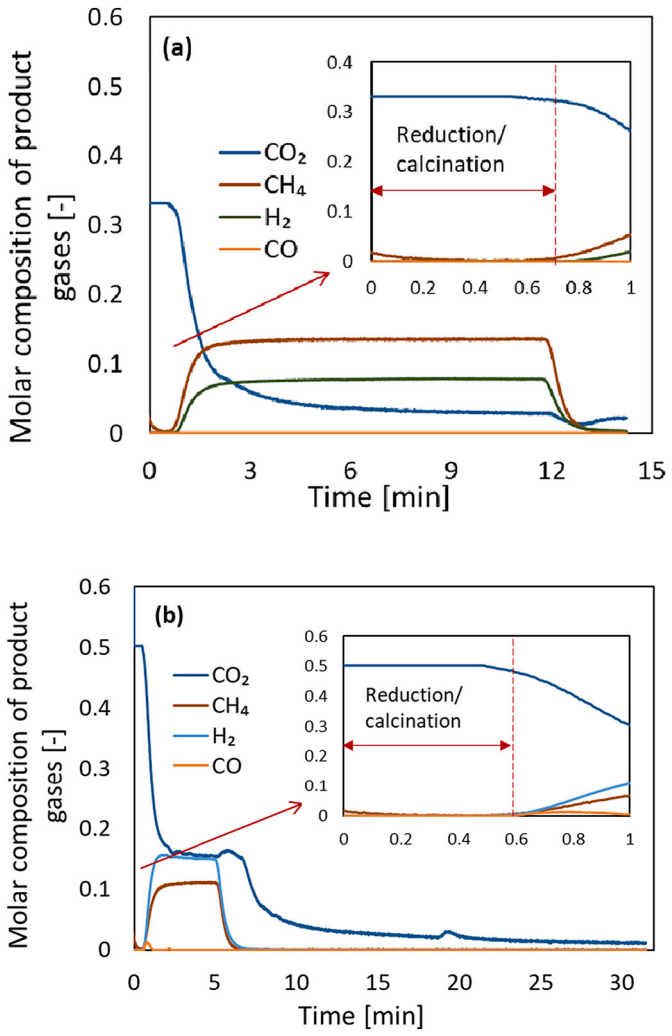

Fig. 18. The molar composition of product gases during the reduction/calcination stage under the operating conditions of a) 800 °C, 1.0 bar, 20% CH_4, 80% N_2 and S/CH_4 molar ratio of 3.0 in the feed (CASE 1); and b) 870 °C, 1.0 bar, 20% CO_2, 20% CO, 20% CH_4, 40% N_2 and S/CH_4 molar ratio of 3.0 in the feed (CASE 2).

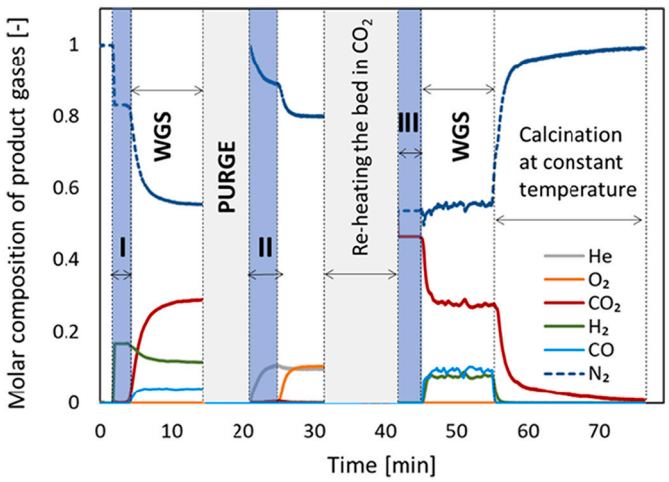

Fig. 19. Product gas evolution with time for an Oxidation, Reduction/Calcination and CASOH stage. The figure includes intermediate heating and cooling steps. (I: CASOH stage; II: Oxidation stage; III: Reduction/calcination stage).

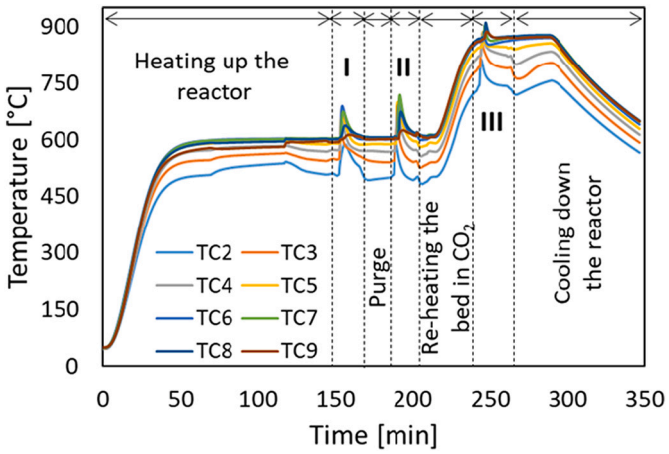

Fig. 20. Temperature profile of one complete cycle of CASOH process (I: CASOH stage; II: Oxidation stage; III: Reduction/calcination stage).

4.6. Complete cycle

The composition of product gases at the exit of reactor during each stage is shown in Fig. 19. As discussed earlier, CASOH stage involves the production of H_2-rich stream (17% H_2 on dry basis). H_2-rich stream is intended as a gas that would be substantially pure H_2 (>99%) on dry and N_2 free basis. The CO_2 captured in CASOH stage is mainly released during the regeneration stage as CaO-based sorbent is regenerated by the calcination of $CaCO_3$. In the regeneration stage, the outlet gas rich in CO_2 (46% CO_2 and 54% N_2) would necessitate an additional capture step. This could be possible by employing CO_2/N_2 adsorption process or cryogenic separation.

Fig. 20 shows the one complete CASOH cycle temperature profile starting from heating the bed to the cooling down the reactor after the reduction/calcination stage under the optimum operating conditions for each stage in the CASOH process.

At the end of the experimental campaign, the structural characterization of the Ca—Cu material after the different stages in the CASOH process is observed using the Scanning Electron Microscopy (SEM) data for the fresh and spent materials (Ca-based and Cu based material). The SEM images of fresh and spent Cu material show that there is a change in the structure of Cu material after multiple cycles of CASOH process. The overall surface area of Cu material has increased as can be seen in more magnified images as shown in Fig. 21.

On the other hand, the SEM images of fresh and spent Ca-based material show that there is no change in the structure of the material after multiple cycles of CASOH process as shown in the Fig. 22.

5. Conclusion

In this paper, the three main reaction stages of the process were examined under the various operating conditions of temperature, pressure, flowrate and feed composition. The results show that the system CaO/CuO is capable of converting a gas with typical BFG composition in a H_2/N_2 gas stream (H_2/N_2: 17%/82%, <1% unconverted CO and leakage of CO_2) under the operating conditions of 600 °C feed temperature, 5.0 bar and S/CO of 2.0. The maximum temperature attained during the Cu-oxidation stage can be restricted below 700 °C, which causes only 3.5% calcination of the $CaCO_3$ available in the bed. The calcination of $CaCO_3$ increases from 3.5% to 8.0% as the initial solids bed temperature increases from 600 °C to 650 °C at 5.0 bar operating pressure. The amount of CO_2 released during the oxidation increases from 0.6% vol. to 1.6% vol. with the decrease in pressure from 5.0 bar to 1.0 bar. The regeneration stage is carried out with different gases available in a steel mill and is expected to lead to a complete calcination

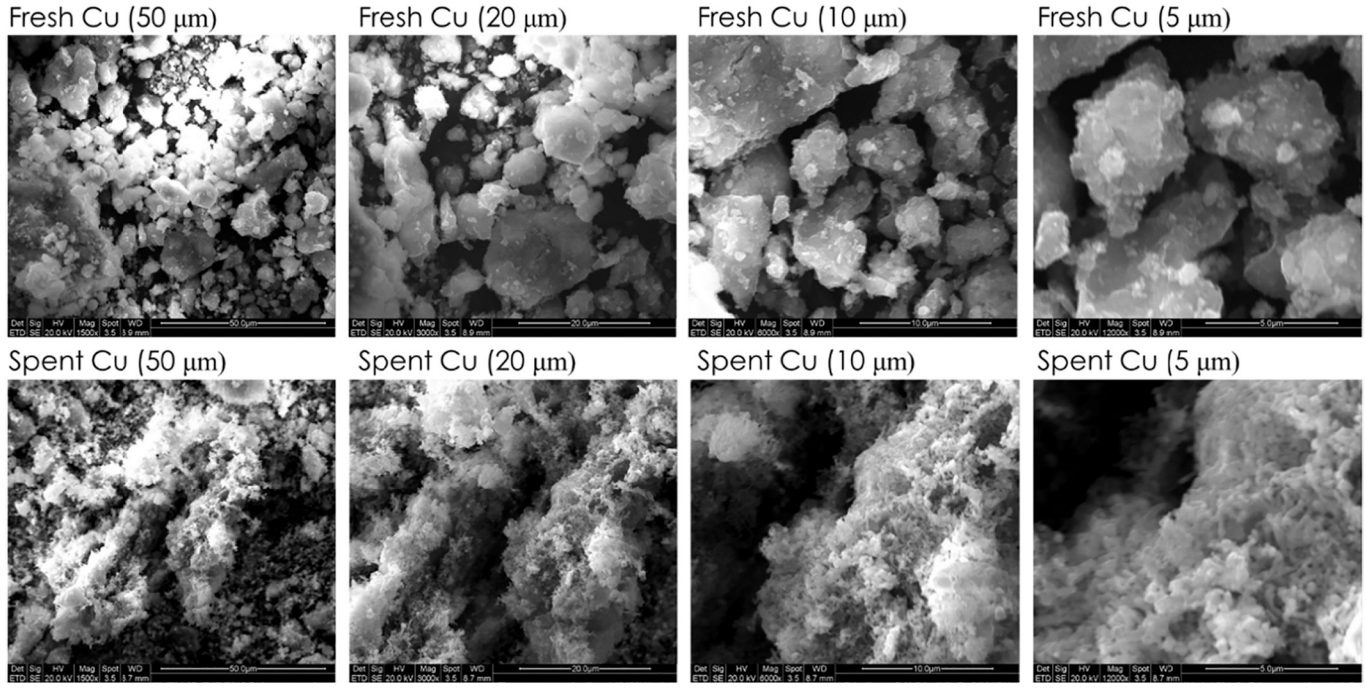

Fig. 21. SEM images of fresh and spent Cu-based material.

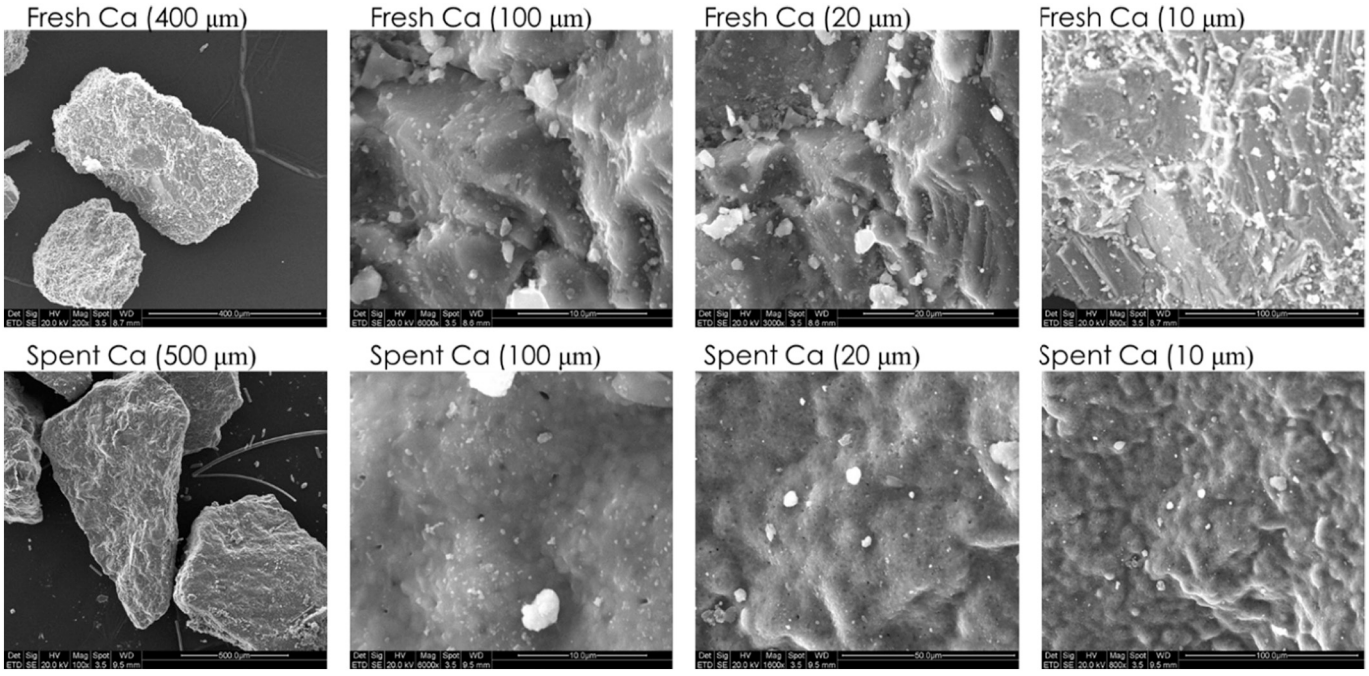

Fig. 22. SEM images of fresh and spent Ca-based material.

of the $CaCO_3$ present in the bed, giving as product a gas with different CO_2 content. The CuO reduction, using BFG, at 800 °C, 850 °C and 870 °C causes 10%, 50% and 80% calcination of $CaCO_3$ respectively. This shows a temperature higher than 850 °C is preferable for the sorbent regeneration. The CO_2 content starting from 46% diluted in N_2 (on dry basis) in case of only BFG at 870 °C, 33% in **CASE 1** (20% CH_4 and 80% N_2 in feed) at 800 °C and 50% CO_2 in **CASE 2** (20% CO, 20% CO_2, 20% CH_4 and 40% N_2 in feed). This makes necessary a subsequent purification of CO_2 in a CPU unless a N_2-free fuel such as NG is used. In terms of energy outputs, the results demonstrate that it is possible to convert a low quality BFG stream into a H_2 rich gas and pure CO_2 stream with a very low energy penalty.

CRediT authorship contribution statement

Syed Zaheer Abbas: Conceptualization, Methodology, Software, Writing – original draft, Investigation, Formal analysis, Validation. **José Ramón Fernández:** Conceptualization, Methodology, Writing – review & editing. **Alvaro Amieiro:** Resources, Writing – review & editing. **Monisha Rastogi:** Resources, Writing – review & editing. **Johan**

Brandt: Resources, Writing – review & editing. **Vincenzo Spallina:** Supervision, Project administration, Conceptualization, Methodology, Writing – review & editing, Funding acquisition.

Declaration of Competing Interest

The authors declare that they have no known competing financial interests or personal relationships that could have appeared to influence the work reported in this paper.

Data availability

Data will be made available on request.

Acknowledgements

The work has received funding from the European Union's Horizon 2020 research and innovation programme under grant agreement no. 884418 (C^4U project). The work reflects only the authors' views and the European Union is not liable for any use that may be made of the information contained therein. The authors acknowledge the financial support from the EPSRC BREINSTORM project, EP/S030654/1. The authors would like to acknowledge Yash Bansod from the University of Manchester for carrying out the SEM analyses of the samples.

References

[1] Worldsteel Association, World Steel Organisation. https://www.worldsteel.org/en/dam/jcr:96d7a585-e6b2-4d63-b943-4cd9ab621a91/World%2520Steel%2520in%2520Figures%25202019.pdf, 2018.
[2] IPCC, IPCC, 2021: Climate Change 2021: The Physical Science Basis. Contribution of Working Group I to the Sixth Assessment Report of the Intergovernmental Panel on Climate Change, 2021.
[3] M. Yellishetty, P.G. Ranjith, A. Tharumarajah, Iron ore and steel production trends and material flows in the world: is this really sustainable? Resour. Conserv. Recycl. 54 (2010) 1084–1094.
[4] D.E. Wiley, M.T. Ho, A. Bustamante, Assessment of opportunities for CO2 capture at iron and steel mills: an Australian perspective, Energy Procedia 4 (2011) 2654–2661.
[5] N. McQueen, C.M. Woodall, P. Psarras, J. Wilcox, CCS in the iron and steel industry, in: Carbon Capture and Storage, Royal Society of Chemistry, 2019, pp. 353–391.
[6] M. Gazzani, M.C. Romano, G. Manzolini, CO2 capture in integrated steelworks by commercial-ready technologies and SEWGS process, Int. J. Greenhouse Gas Control. 41 (2015) 249–267.
[7] A. Arasto, E. Tsupari, J. Kärki, E. Pisilä, L. Sorsamäki, Post-combustion capture of CO2 at an integrated steel mill–part I: Technical concept analysis, Int. J. Greenhouse Gas Control. 16 (2013) 271–277.
[8] E. Tsupari, J. Kärki, A. Arasto, E. Pisilä, Post-combustion capture of CO2 at an integrated steel mill–Part II: economic feasibility, Int. J. Greenhouse Gas Control. 16 (2013) 278–286.
[9] M.C. Romano, P. Chiesa, G. Lozza, Pre-combustion CO2 capture from natural gas power plants, with ATR and MDEA processes, Int. J. Greenhouse Gas Control. 4 (2010) 785–797.
[10] M. Dreillard, P. Broutin, P. Briot, T. Huard, A. Lettat, Application of the DMXTM CO2 capture process in steel industry, Energy Procedia 114 (2017) 2573–2589.
[11] M. Lacroix, P. Broutin, S. Lethier, D. Nevicato, B. Petetin, E. De Coninck, X. Courtial, I.F.P. TOTAL, A. ArcelorMittal, DMX demonstration in dunkirk: 3D projects granted by H2020: scope and objectives, in: TCCS-10 Conference, Trondheim, Norway, 2019.
[12] P. Broutin, B. Petetin, X. Courtial, M. Lacroix, 3D: A H2020 Project for the Demonstration of the DMXTM Process, Oral Presentation at PCCC-5, Kyoto, 2019.
[13] G. Ji, J.G. Yao, P.T. Clough, J.C.D. Da Costa, E.J. Anthony, P.S. Fennell, W. Wang, M. Zhao, Enhanced hydrogen production from thermochemical processes, Energy Environ. Sci. 11 (2018) 2647–2672.
[14] E.R. Van Selow, P.D. Cobden, P.A. Verbraeken, J.R. Hufton, R.W. Van den Brink, Carbon capture by sorption-enhanced water– gas shift reaction process using hydrotalcite-based material, Ind. Eng. Chem. Res. 48 (2009) 4184–4193.
[15] A. Arasto, E. Tsupari, J. Kärki, M. Sihvonen, J. Lilja, Costs and potential of carbon capture and storage at an integrated steel mill, Energy Procedia 37 (2013) 7117–7124.
[16] Á.A. Ramírez-Santos, C. Castel, E. Favre, Utilization of blast furnace flue gas: opportunities and challenges for polymeric membrane gas separation processes, J. Membr. Sci. 526 (2017) 191–204.
[17] H. Saima, Y. Mogi, T. Haraoka, Development of PSA technology for the separation of carbon dioxide from blast furnace gas, in: JFE Technical Report, 2014, pp. 133–138.
[18] J.R. Fernández, I. Martínez, J.C. Abanades, M.C. Romano, Conceptual design of a Ca–Cu chemical looping process for hydrogen production in integrated steelworks, Int. J. Hydrog. Energy 42 (2017) 11023–11037.
[19] S. Tian, K. Li, J. Jiang, X. Chen, F. Yan, CO2 abatement from the iron and steel industry using a combined Ca–Fe chemical loop, Appl. Energy 170 (2016) 345–352.
[20] D.P. Harrison, Sorption-enhanced hydrogen production: a review, Ind. Eng. Chem. Res. 47 (2008) 6486–6501.
[21] C.S. Martavaltzi, E.P. Pampaka, E.S. Korkakaki, A.A. Lemonidou, Hydrogen production via steam reforming of methane with simultaneous CO2 capture over CaO– Ca12Al14O33, Energy Fuel 24 (2010) 2589–2595.
[22] Y. Liu, Z. Li, L. Xu, N. Cai, Effect of sorbent type on the sorption enhanced water gas shift process in a fluidized bed reactor, Ind. Eng. Chem. Res. 51 (2012) 11989–11997.
[23] J.R. Fernández, J.C. Abanades, R. Murillo, G. Grasa, Conceptual design of a hydrogen production process from natural gas with CO2 capture using a Ca–Cu chemical loop, Int. J. Greenhouse Gas Control. 6 (2012) 126–141.
[24] J.R. Fernández, J.C. Abanades, Optimized design and operation strategy of a CaCu chemical looping process for hydrogen production, Chem. Eng. Sci. 166 (2017) 144–160.
[25] S.S. Kazi, A. Aranda, L. Di Felice, J. Meyer, R. Murillo, G. Grasa, Development of cost effective and high performance composite for CO2 capture in Ca-Cu looping process, Energy Procedia 114 (2017) 211–219.
[26] L. Riva, I. Martínez, M. Martini, F. Gallucci, M. van Sint Annaland, M.C. Romano, Techno-economic analysis of the Ca-Cu process integrated in hydrogen plants with CO2 capture, Int. J. Hydrog. Energy 43 (2018) 15720–15738.
[27] I. Martínez, M. Martini, L. Riva, F. Gallucci, M.V.S. Annaland, M.C. Romano, Techno-economic analysis of a natural gas combined cycle integrated with a Ca-Cu looping process for low CO2 emission power production, Int. J. Greenhouse Gas Control. 81 (2019) 216–239.
[28] J.R. Fernández, J.C. Abanades, Overview of the Ca–Cu looping process for hydrogen production and/or power generation, Curr. Opin. Chem. Eng. 17 (2017) 1–8.
[29] M. Martini, M. Druiff, M. van Sint Annaland, F. Gallucci, Experimental demonstration of the Ca-Cu looping process, Chem. Eng. J. 418 (2021), 129505.
[30] I. Martínez, J.R. Fernández, M. Martini, F. Gallucci, M. van Sint Annaland, M. C. Romano, J.C. Abanades, Recent progress of the Ca-Cu technology for decarbonisation of power plants and carbon intensive industries, Int. J. Greenhouse Gas Control. 85 (2019) 71–85.
[31] I. Martínez, J.R. Fernández, J.C. Abanades, M.C. Romano, Integration of a fluidized-bed Ca-Cu chemical looping process in a steel mill, Energy. 163 (2018) 570–584, https://doi.org/10.1016/J.ENERGY.2018.08.123.
[32] J.R. Fernandez, V. Spallina, J.C. Abanades, Advanced packed-bed Ca-Cu looping process for the CO 2 capture from steel mill off-gases, Front. Energy Res. 8 (2020) 146.
[33] M. Martini, A. van Den Berg, F. Gallucci, M. van Sint Annaland, Investigation of the process operability windows for Ca-Cu looping for hydrogen production with CO2 capture, Chem. Eng. J. 303 (2016) 73–88.
[34] M.A. San Pio, M. Martini, F. Gallucci, I. Roghair, M. van Sint Annaland, Kinetics of CuO/SiO2 and CuO/Al2O3 oxygen carriers for chemical looping combustion, Chem. Eng. Sci. 175 (2018) 56–71.
[35] L. Díez-Martín, G. Grasa, R. Murillo, M. Martini, F. Gallucci, M. van Sint Annaland, Determination of the oxidation kinetics of high loaded CuO-based materials under suitable conditions for the Ca/Cu H2 production process, Fuel. 219 (2018) 76–87.
[36] Y. Yan, V. Manovic, E.J. Anthony, P.T. Clough, Techno-economic analysis of low-carbon hydrogen production by sorption enhanced steam methane reforming (SE-SMR) processes, Energy Convers. Manag. 226 (2020), 113530.
[37] Y. Yan, K. Wang, P.T. Clough, E.J. Anthony, Developments in calcium/chemical looping and metal oxide redox cycles for high-temperature thermochemical energy storage: a review, Fuel Process. Technol. 199 (2020), 106280.
[38] C.C. Dean, J. Blamey, N.H. Florin, M.J. Al-Jeboori, P.S. Fennell, The calcium looping cycle for CO2 capture from power generation, cement manufacture and hydrogen production, Chem. Eng. Res. Des. 89 (2011) 836–855.
[39] F. Donat, N.H. Florin, E.J. Anthony, P.S. Fennell, Influence of high-temperature steam on the reactivity of CaO sorbent for CO2 capture, Environ. Sci. Technol. 46 (2012) 1262–1269.
[40] J. Boon, V. Spallina, Y. van Delft, M. van Sint Annaland, Comparison of the efficiency of carbon dioxide capture by sorption-enhanced water–gas shift and palladium-based membranes for power and hydrogen production, Int. J. Greenhouse Gas Control. 50 (2016) 121–134.
[41] G. Manzolini, A. Giuffrida, P.D. Cobden, H.A.J. van Dijk, F. Ruggeri, F. Consonni, Techno-economic assessment of SEWGS technology when applied to integrated steel-plant for CO2 emission mitigation, Int. J. Greenhouse Gas Control. 94 (2020), 102935.
[42] A.W.D. Hills, Equilibrium decomposition pressure of Calcium carbonate between 700 and 900°C, Inst. Min. Metall. 76 (1967) C241–C245.
[43] J.M. Alarcón, J.R. Fernández, CaCO3 calcination by the simultaneous reduction of CuO in a Ca/Cu chemical looping process, Chem. Eng. Sci. 137 (2015) 254–267.
[44] Innovative industrial transformation of the steel and chemical industries of Europe. https://cordis.europa.eu/project/id/958318, 2022.
[45] From Residual Steel Gases to Methanol. http://www.fresme.eu/, 2022.
[46] Efficient CO2 Conversion Over Multisite Zeolite-Metal Nanocatalysts to Fuels and OlefinS. https://www.spire2030.eu/cozmos, 2022.
[47] G.S. Grasa, J.C. Abanades, CO2 capture capacity of CaO in long series of carbonation/calcination cycles, Ind. Eng. Chem. Res. 45 (2006) 8846–8851.

[48] F. Garcia-Labiano, J. Adánez, L.F. de Diego, P. Gayán, A. Abad, Effect of pressure on the behavior of copper-, iron-, and nickel-based oxygen carriers for chemical-looping combustion, Energy Fuel 20 (2006) 26–33.
[49] A. Abad, J. Adánez, F. García-Labiano, F. Luis, P. Gayán, J. Celaya, Mapping of the range of operational conditions for Cu-, Fe-, and Ni-based oxygen carriers in chemical-looping combustion, Chem. Eng. Sci. 62 (2007) 533–549.
[50] J.R. Fernández, J.M. Alarcón, J.C. Abanades, Study of the calcination of CaCO3 by means of a Cu/CuO chemical loop using methane as fuel gas, Catal. Today 333 (2019) 176–181.